Encapsulating Ion-Solid Interactions in Metal-Oxide-Semiconductor (MOS) Devices

Radhey Shyam, Dhruva D. Kulkarni, Daniel A. Field, Endu S. Srinadhu, James E. Harriss, William R. Harrell, and Chad E. Sosolik

***Abstract*—We report on a measurement of low energy ion irradiation effects on as-grown films of SiO_2 on a Si substrate. Beams of normally incident Na^+ ions with kinetic energies of 2 keV to 5 keV were focused onto $\sim$ 1900 Å SiO_2 films. Aluminum top metal contacts were subsequently deposited onto these targets such that irradiated regions and unexposed (pristine) regions of the target could be compared using capacitance–voltage (C–V) measurements of individual metal-oxide-semiconductor (MOS) devices. The C–V data reveal an energy-dependent shift in the flatband voltage (V_{FB}) that can be returned to its near-pristine value by a low temperature anneal. An increase in the density of interface states (D_{it}) inferred from the C–V curves is found to have a superlinear dependence on the incident kinetic energy. These data are consistent with previously observed UV radiation effects on MOS oxides, where transferred energy leads to electron-hole pair production and the diffusion and trapping of holes throughout the oxide. Our measured trapped hole densities are compared with calculated densities, which are based on the incident ion dose and the predicted ion implantation range, to arrive at a fractional yield for hole survival and measurement within an encapsulated MOS device.**

***Index Terms*—Electron-hole pairs, hole-trapping, interface traps, ion beams, ion implantation, ion radiation effects, linear energy transfer, metal-oxide-semiconductor (MOS) devices, radiation damage.**

I. Introduction

EXPERIMENTAL measurements of the effects of low energy ion irradiation on insulating solids can be challenging to interpret, as the primary probe, atomic force microscopy, is a top layer specific technique [1], [2]. In this paper, we demonstrate that irradiation effects from ions can be probed after an insulator is encapsulated into a finished metal-oxide-semiconductor (MOS) device. Specifically, by measuring capacitance–voltage (C–V) of the MOS structure we can resolve the residue of energy-dependent electron-hole pair excitations induced by the passage of ions into the subsurface of the previously exposed insulator.

In our previous work on encapsulation of irradiation effects, we were able to show that crater formation on a thin film dielectric (Al_2O_3) can be probed in a metal-insulator-metal (MIM) device [3]. Each device was probed using differential conductance measurements through films that had been exposed to highly charged ions, and the conductance change per ion impact was interpreted as a single ion effect dependent on charge state. In this work we focus on singly-charged ions which are embedded near the surface of an oxide film. The unique sensitivity of an MOS device to interstitial ions and trapped charge effects through C–V measurements [4] is then exploited to explore how the kinetic energy of the stopped ions was dissipated.

Studies of the dependence of MOS device performance on radiation damage have a long history in the context of applied device physics [5]–[10] given their relevance to fabrication-induced effects, such as those arising from the passage of dopant ions through the oxide and bound for the underlying semiconductor substrate [11]–[16]. To understand these effects as well as those arising in deployed MOS devices, i.e., devices in harsh radiation-intensive environments, numerous investigations have employed intentional sources of radiation damage, such as gamma rays [5], [6], high energy ions [6], [7], [9], [10], and UV sources [17]. It is from these experiments that a detailed picture was developed for oxide radiation damage in MOS structures, incorporating data on depth, time, and voltage-dependent observations. In the context of applied devices, however, the transition of MOS and MOSFET structures to ever thinner oxides has diminished the role that radiation damage plays in state-of-the-art device performance [10]. In contrast, for the work we present here, we intentionally utilize thicker oxide layers to show that their inherent sensitivity to radiation damage allows ions with shallow implantation depths to give rise to significantly shifted C–V signatures that are linked to inelastic energy losses within the oxide.

The organization of this paper is as follows. In Section II we describe our MOS device fabrication and characterization both pre- and post-irradiation with low energy Na^+ ions. Results for irradiated devices are discussed in Section III and compared with a phenomenological model based on ion stopping values extracted from SRIM [18]. Conclusions from these data are summarized in Section IV.

II. Experiment

Our MOS devices were fabricated in-house at Clemson University. The starting materials were 3-in p-type Si(100) wafers

Manuscript received May 29, 2015; revised September 04, 2015; accepted October 06, 2015. Date of current version December 11, 2015. This work was supported in part by the National Science Foundation under Grant NSF-DMR-0960100, by DARPA under ARO Grant W911NF-13-1-0042) and by the Clemson University College of Engineering and Science. *(Radhey Shyam and Dhruva D. Kulkarni contributed equally to this work.)*

R. Shyam, D. D. Kulkarni, D. A. Field, E. S. Srinadhu, J. E. Harriss, and C. E. Sosolik are with the Department of Physics and Astronomy, Clemson University, Clemson, SC 29634 USA (e-mail: sosolik@clemson.edu).

W. R. Harrell is with the Holcombe Department of Electrical and Computer Engineering, Clemson University, Clemson, SC 29634 USA.

Color versions of one or more of the figures in this paper are available online at http://ieeexplore.ieee.org.

Digital Object Identifier 10.1109/TNS.2015.2489468

purchased from Silica-Source, Inc. The wafers, which had resistivities of $1-10\,\Omega-$cm, were precleaned to remove organic surface contaminants prior to oxide growth. The cleaning procedure was a standard RCA clean (1:1:5 solution of $NH_4OH + H_2O_2 + H_2O$) for five minutes under ultrasonic agitation. The cleaned surface was then etched with dilute 1% hydrofluoric acid for two minutes to remove any native oxide followed by a triple rinse in deionized water for a total of six minutes.

Oxide was grown on the samples by placing them in an oxidation furnace for 25 min at 1000°C under a steam flow. Measurements of the resulting film thickness with a Nanometrics NanoSpec AFT (Automatic Film Thickness) gave a nominal value of 1900 Å (1887 Å $\pm$ 43 Å). Preparation of the wafer backside involved etching with concentrated hydrofluoric acid to remove the grown oxide, triple-rinsing with deionized water and subsequent deposition of 0.5 μm of Al from a thermal evaporator. The as-deposited Al contacts were sintered at 450°C for 30 min in a nitrogen environment. Finally, the wafers were diced into 12 mm $\times$ 12 mm squares to accomodate the sample mount for our ion irradiation setup.

Sample irradiations were carried out using Na^+ ions obtained from an aluminosilicate emitter (Heatwave Tech) mounted in a custom-built ion source. The oxidized and diced Si wafer targets were mounted directly in front of this source in the first section of our ion beamline, which is described in detail elsewhere [19]. The plate holding each target was masked so that only a central circular region ($\sim$ 6 mm diameter) would be exposed to the incident ions. Prior to each irradiation, an initial beam tuning was obtained by focusing the beam through an aperture that was equivalent in size to the central mask and into a Faraday cup mounted directly behind the sample position. Ion doses in the 10^{12} ions $\cdot$ cm^{-2} range with incident energies between 2 and 5 keV were used. Beam profiles were obtained using a beam viewer located directly behind the Faraday cup. The base pressure within the beamline during irradiations was 6.67×10^{-5} Pa. After each irradiation, the target was removed from the beamline so that MOS top contacts of Al could be deposited. For these depositions, a custom-built mask was used which placed four Al top contacts in the central, irradiated region and four Al top contacts in the corner, unirradiated regions of the target. This gave eight MOS devices per target (four irradiation-encapsulated and four pristine). We note that the deposition, which occurred at a pressure of 1.33×10^{-4} Pa, led to a sample frontside temperature no higher than 80°C, as based on prior characterization measurements. Fig. 1 shows the devices obtained after deposition with reference to the area exposed to the beam.

Both pristine and irradiated devices were characterized using C–V measurements. A micromanipulator probe station connected to a HP4280A for high frequency (HF) measurements and a HP4140B for low frequency (LF) measurements was used to obtain the C–V characteristics of each individual MOS device. The HF measurements were carried out at 1 MHz while the LF measurements were carried out in a quasi-static manner resulting in a frequency less than 10 Hz. The variation in typical LF and HF signatures of one of our irradiated MOS capacitors as compared to a pristine MOS capacitor is shown in Fig. 2. The pristine device C–V signature is shown by lighter curves while the dark curves are the signature of the irradiated device.

Fig. 1. Typical beam profile, obtained on analyzing images from a beam viewer placed behind the irradiation mask for 3 keV Na^+ ions, superimposed on an image of an Omicron-style sample holder showing the four centrally located irradiated devices and the four pristine devices at the corners. The color scale indicates intensity of an illuminated pixel in the beam viewer image used to obtain the profile. For this measurement, the beam current measured through an aperture of $\sim$ 6 mm diameter was 12.33 nA.

As a function of the applied gate voltage, both the LF and HF C–V curves show accumulation behavior at the most negative applied voltages and hence give similar capacitance values due to the intrinsic capacitance of the 1900 Å oxide layer. For the LF C–V this result is mirrored at the most positive applied gate voltage where the MOS device goes into inversion whereas the HF C–V is lower due to the capacitance of the depletion layer. Between these two extremes, both LF and HF C–V curves for the pristine device show a distinct drop at a point in voltage that is near to the so-called flatband voltage ($V_{\rm FB}$) where, for an ideal system, the applied gate voltage equals the difference in work function between the Al gate and the Si substrate ($\approx$ 0.8 eV). This flatband voltage is identified in our experiment as the voltage at which the capacitance is 0.91 times the maximum capacitance of the oxide [20]. More generally, however, $V_{\rm FB}$ can be considered as sensitive to the detailed conditions of the oxide and its interfaces and, in particular, to implanted charged species and any additional charges, such as excited holes, left by irradiation. For example, the 3 keV Na^+ irradiated device in Fig. 2 shows a significant shift in the $V_{\rm FB}$ position. Another feature of the data is the increased skew of the irradiated C–V curve as compared to the pristine curve, as shown by the dash-dot line in Fig. 2, which is related to an increase in the interface trap density, $D_{\rm it}$. Therefore, it is through the shifted flatband voltage, ($\Delta V_{\rm FB}$), and the increase in interface trap density, $D_{\rm it}$, that we track the energetics of kinetic energy dissipation for our Na^+ ions within the MOS oxide layer.

III. Results and Discussion

For this study, we irradiated our as-prepared SiO_2 ($\approx$ 1900 Å) targets with beams of Na^+ ions that had energies between 2 and 5 keV. All target doses were in the range of $6-8\times10^{12}$ ions $\cdot$ cm^{-2}. Following each irradiation, Al top

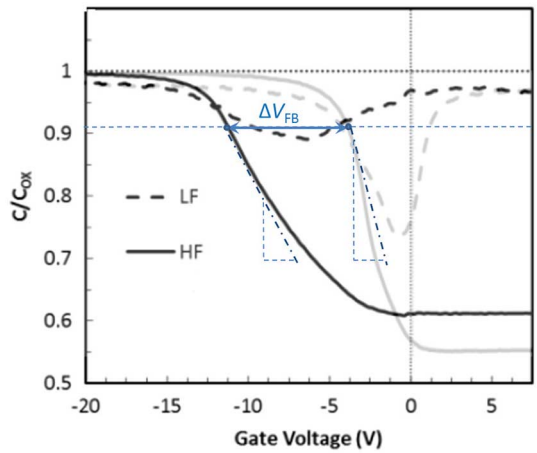

Fig. 2. C–V signatures (LF and HF) for typical pristine (lighter curves) and a device irradiated with 3 keV Na^+ ions(darker curves). The shift in the flatband voltage, $\Delta V_{\rm FB}$, is calculated as the difference in the voltage where the capacitance is 0.91 times the max capacitance value. The illustrated change in the slope of the C–V curves, or equivalently the increased voltage range between accumulation and inversion, indicates an increase in the interface trap density $D_{\rm it}$.

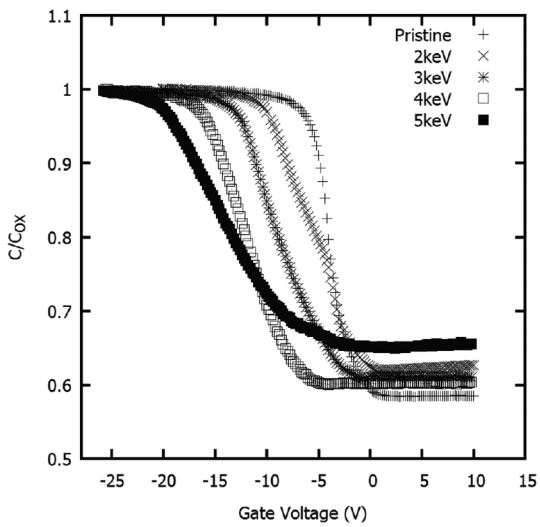

Fig. 3. Irradiated device CV curves (HF) for devices exposed to Na^+ ions in the range of 2–5 keV. The capacitance values have been normalized by $C_{\rm ox}$.

contacts were deposited as noted in Section II and the finished MOS devices were characterized by C–V measurements. Representative C–V data for four devices in the irradiated energy range are shown in Fig. 3. It is clear from these spectra that there is a significant shift in the position of the flatband toward more negative gate voltage values as the incident beam energy is increased. Additionally, we note that the shift is not a parallel shift but includes stretching out the C–V curve. Our results showing $\Delta V_{\rm FB}$ for irradiated target regions are summarized in Fig. 5. The devices constructed on the masked or unirradiated regions of the targets, not shown in the figure, have a nearly constant value of ~ -3.8 V across all samples. This reproducible value served as a consistency check on our fabrication technique, and we attribute the shift away from the

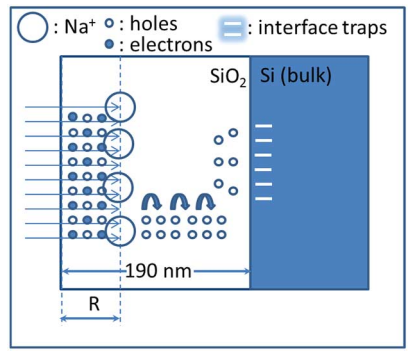

Fig. 4. Schematic depicting hole creation and transport in the oxide leading to a shift in the flatband voltage and skew in the C–V curve. See text for details.

ideal value of -0.8 V to the trapping of positive charge during the fabrication process [20].

Fig. 4 schematically depicts the processes occurring as a consequence of the irradiation that lead to a shift in the flatband voltage and also to creation of radiation-induced interface traps. The large unfilled circles represent the implanted Na^+ ions. The mean depth of implantation, or range "R," of these incident ions is expected, via simulations, to be less than 12 nm. As these ions remain in the charged state in the oxide, it is reasonable to expect a flatband shift due to the ions themselves. However, the shift expected due to the ions themselves is only approximately a third to a fourth of the measured flatband shift. The additional shift is attributed to the creation of holes due to electron-hole pair excitation along the short track of these ions. Electrons are depicted by filled circles while holes are depicted by small unfilled circles. Most of these electron-hole pairs recombine, however, a fraction ($\sim 1\%$) escape recombination.

The electrons that escape recombination are swept away due to their high mobility and do not contribute further to the radiation-response of the MOS structure; however, the surviving holes, having a mobility many orders of magnitude lower than the electrons, are trapped in the oxide. These trapped holes undergo a stochastic hopping transport through the oxide, activated by internal electric fields of the ions themselves and possibly internal contact potentials, and migrate towards the semiconductor interface where they are trapped in deep trapping sites, and can remain trapped for a period ranging from hours to years. This additional positive charge trapped in the oxide leads to the observed additional shift in the C–V curve of the MOS capacitor. This shift has been observed to persist for a period of at least one year for our devices.

Imperfections, due to imbalance in the proportion of silicon and oxygen, are always present in the interface between the oxide and semiconductor leading to dangling silicon bonds or equivalently the so-called interface traps. The energy levels of these traps lie within the bandgap and their occupancy depends on the Fermi level, and consequently, on the applied gate voltage. In addition to the flatband shift, post-irradiation response of the MOS devices also shows an increased skew, or distortion, in the C–V curves as compared to the pristine curves. Thus we infer that radiation-induced interface traps were created as a result of ion irradiation.

The shift and skew in the C–V curves of the MOS devices thus represents the energy lost by the impacting ions to electronic excitations within the oxide. The ions themselves are implanted in the first $\sim$ 10 nm; however, carrier transport in the oxide results in interface-trapped states at the $Si-SiO_2$ interface $\sim$200 nm away from the implanted ions. As the flatband shift depends on the first moment of the charge trapped in the oxide, the MOS structure is inherently sensitive to radiation damage, which consequently results in a measurable signal in terms of the flatband shift and creation of interface states. Thus, MOS devices can be a useful tool for measuring energy loss of low energy ions in dielectric films, which is otherwise experimentally refractory. In the remainder of this section, we explore quantitatively the energy dependence of the voltage shift and also the increase in populated interface trap density.

For the irradiated devices, the measured $\Delta V_{\rm FB}$ values shown in Fig. 5 lie between approximately -4 V and -14 V and increase monotonically across the incident Na^+ kinetic energy range. In general, $\Delta V_{\rm FB}$ in MOS devices can be attributed to the presence of charges in the oxide and is given by [21]

$$\Delta V_{\rm FB} = \frac{1}{C_{\rm ox} x_{\rm ox}} \int_0^{x_{\rm ox}} \rho(x) x \mathrm{d}x \tag{1}$$

where $\rho(x)$ is the charge distribution within the oxide, $C_{\rm ox}$ is the maximum capacitance of the oxide per unit area, x is distance within the oxide measured from the metal-oxide interface and $x_{\rm ox}$ is the thickness of the oxide. From (1) it is clear that observed shifts in $V_{\rm FB}$ are proportional to the amount of charge present in the oxide. For the parameters of these measurements (Na^+ kinetic energy and oxide thickness) it is reasonable to assume that the incident ions penetrate into and are implanted within the oxide. Additionally, Na^+ ions are known to remain ionized inside SiO_2[13]. Therefore, some fraction of the $V_{\rm FB}$ shifts we observe could be assigned to the presence of implanted ions in the oxide. Since (1) also indicates that $V_{\rm FB}$ shifts will depend on the depth of the charge in the oxide, it is possible that ions of higher kinetic energy, which will travel further into the oxide, could give rise to shifts in $V_{\rm FB}$ that are tied to the implantation depth and its kinetic energy dependence. In order to estimate the contribution of the Na^+ ions and their depth within the oxide to our measured $V_{\rm FB}$ values, the Monte Carlo code SRIM [18] was used. SRIM is a collection of well known and widely used computer codes which calculate the stopping range of heavy ions in matter along with related effects such as sputtering, recoils, and damage. Relevant results from SRIM are shown in Table I. The depth profile of the implanted ions obtained from SRIM was Gaussian ($G_{\mu,\sigma}(x)$) in shape, where the mean implantation depth, μ, ranged between 5.9 and 11.8 nm with a standard deviation, σ, between 2.8 and 5.5 nm. Substituting this distribution for the charge distribution $\rho(x)$ in (1), we find an estimated contribution of the implanted ions to $V_{\rm FB}$ which is plotted in Fig. 5. A linear fit to the measured flatband shift resulted in a slope of 3.0 ± 0.2 V/keV, while a slope of 0.8 ± 0.1 V/keV was obtained for the calculated shift resulting from only the ions themselves. Relative to the measured $V_{\rm FB}$ values at each kinetic energy, we see from the slopes of the linear fit that the implanted ions contribute no more than $\sim 25\% - 30\%$ of the total $V_{\rm FB}$. Therefore, the observed linear

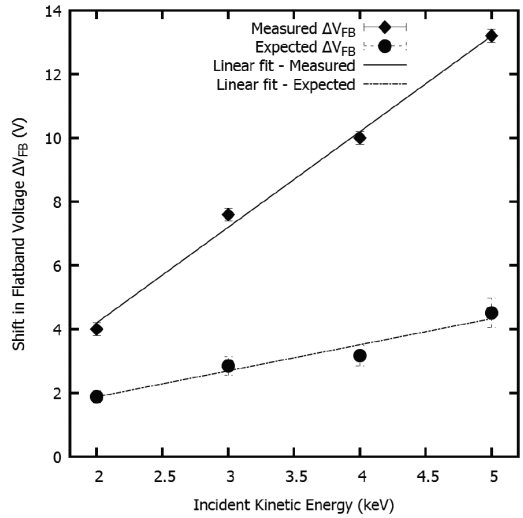

Fig. 5. Measured flatband voltage shifts $\Delta V_{\rm FB}$ for irradiated (♦) MOS devices, plotted with respect to the incident energy of the Na^+ ions. The measured shifts were negative, absolute values are plotted for clarity. The expected contribution of the implanted Na^+ ions to the overall flatband shift is also plotted (•) and was determined using the experimental ion dose and device area along with depth profiles obtained from SRIM. Linear fits to the measured and expected contribution result in slopes of 3.0 ± 0.2 V/keV and 0.8 ± 0.1 V/keV, respectively.

TABLE I
TABULATED OUTPUT FROM SRIM SHOWING THE RANGE (μ), STRAGGLE (σ) AND ENERGY LOST TO ELECTRONIC EXCITATIONS ($s_{\rm electronic}$) AS A FUNCTION OF KINETIC ENERGY OF THE INCIDENT IONS

Energy(keV)	μ (nm)	σ (nm)	$s_{electronic}$(eV/nm)
2	5.9	2.8	26.5
3	7.9	3.8	32.5
4	9.9	4.7	37.5
5	11.8	5.5	42.0

trend in $V_{\rm FB}$ with respect to kinetic energy cannot be fully accounted for by considering only the contribution of the Na^+ and their depth within the oxide.

To account for the additional shift in $V_{\rm FB}$ that cannot be attributed to the implanted ions themselves, we consider the interactions of the ions with the oxide. In particular, the nuclear and electronic energy loss channels of these ions, typically treated through the stopping power or stopping force ($-dE/dx$), must be considered. It is known that electronic excitations in the oxide above a certain threshold lead to generation of electron-hole pairs, which can appear, post-excitation, as a form of trapped charge that can shift the MOS $V_{\rm FB}$ signature [22]. For the incident ion kinetic energies used in our experiments, the electronic component of stopping power reported by SRIM, as shown in Table I, is in the range of 26.540–41.967 eV/nm. We can calculate the total energy lost to the electronic subsystem of the oxide target per ion as the product of the electronic component of the stopping power ($s_{\rm electronic}$) and the depth of the implanted ion. If we represent the depth through the ion implantation profile $G_{\mu,\sigma}(x)$ obtained from SRIM, the total energy lost to the electronic subsystem per unit area ($\Delta E_{\rm electronic}$) for a given dose d is

$$\Delta E_{\rm electronic} = d s_{\rm electronic} \frac{\int_0^{x_{\rm ox}} x G_{\mu,\sigma}(x) \mathrm{d}x}{\int_0^{x_{\rm ox}} G_{\mu,\sigma}(x) \mathrm{d}x} \tag{2}$$

where the denominator is included as a normalization factor for the Gaussian function. Since it is known that approximately 18 eV is required to generate one electron hole pair in SiO_2[22], we can calculate the number of electron-hole pairs generated per unit area, assuming every electron-hole pair gives rise to a hole in the oxide, as

$$N_{H-SRIM} = \frac{\Delta E_{\text{electronic}}}{18.0}. \tag{3}$$

Although (3) can be used to calculate the density of electron-hole pairs generated in the oxide by the passage of implanted ions, the subsequent recombination and transport of these excitations must be accounted for to determine the final distribution of ion-generated charge. This process is well described by the columnar recombination model developed by Jaffe with subsequent numerical solutions by Oldham [7]–[9]. The model includes terms for diffusion and recombination and is written here as

$$\frac{\partial n_{p,n}}{\partial t} = D_{p,n}\frac{\partial^2 n_{p,n}}{\partial x^2} \mp \mu_{p,n}\mathcal{E}\frac{\partial n_{p,n}}{\partial x} - \alpha n_n n_p \tag{4}$$

where $n_{p,n}$ represents the hole (p) and electron (n) density, $D_{p,n}$ is the diffusion constant, μ is the mobility of the carriers (electron mobility $\mu_n = 40$ cm^2/V-s and hole mobility $\mu_p = 10^{-11}$ cm^2/V-s), $\mathcal{E}$ is electric field resulting from the application of a gate voltage and α is the recombination coefficient. The diffusion constant D scales linearly with the mobility μ according to Einstein's relation. Since the mobilities of the generated electrons and holes vary by multiple orders of magnitude, we can assume that the highly mobile electrons are quickly swept away into the bulk, while the holes require longer to migrate through the oxide. For our experimental setup, with an exposed oxide that has no initial top gates, we can ignore the second term on the right hand side in (4), as there is no field $\mathcal{E}$ due to an applied voltage. We note here that though there is no externally applied electric field, there will be an internal field present due to internal contact potentials and the implanted ions themselves. These internal fields serve to activate hole transport even though there is no externally applied field in our experiment [9].

Under these conditions, the solution to this equation is a uniform distribution of holes that are trapped within the oxide. It is these remaining holes, as trapped positive charge, that give rise to the V_{FB} shifts we observe. Substituting such a uniform distribution into (1), we can determine the $\Delta\, V_{\text{FB}}$ that would have been measured on the irradiated devices on account of these holes (assuming no recombination, i.e., $\alpha = 0$), as

$$\Delta V_{\text{FB}-\text{CALC}} = \frac{eN_{H-SRIM}}{2C_{\text{ox}}}. \tag{5}$$

A comparison between the measured shifts, $\Delta V_{\text{FB}-\text{EXPT}}$ and the calculated shifts, $\Delta V_{\text{FB}-\text{CALC}}$, calculated from kinetic energy induced electronic excitations in the oxide using (5), is shown in Fig. 6. A linear fit to this result gives a slope of 1.2 ± 0.2 which corresponds to a yield of $\sim 1\%$, or equivalently the result that about 1 out of every 100 holes that are generated give rise to the shift we measure in the MOS flatband voltage, while the remainder are lost to recombination and do not contribute to the measured shift. This is compatible with the trends seen in other types of radiation effects [5]–[7], [9], [10] and in particular with UV source results [17]. Moreover, our result is consistent with values found for the recombination coefficent ($\alpha \approx 0.98$) for SiO_2/Si based devices [9].

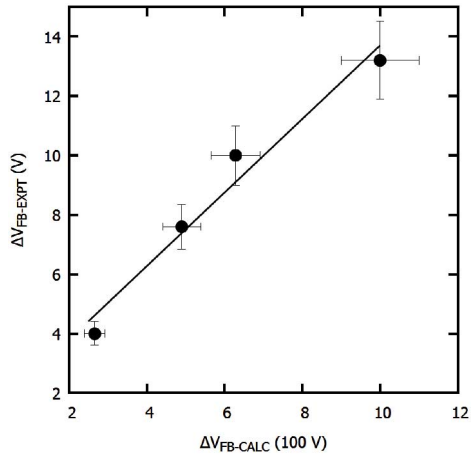

Fig. 6. Calculated $\Delta V_{\text{FB}-\text{CALC}}$ assuming no recombination plotted with the measured flatband shifts, $\Delta V_{\text{FB}-\text{EXPT}}$. The slope obtained by a linear fit (1.2 ± 0.2) is a measure of the holes lost to recombination.

The microscopic mechanism of transport of holes within the oxide is described accurately using a continuous-time-random-walk (CTRW) model [23]. The CTRW describes the time dispersion of holes within an oxide with a single value of the disorder parameter, which implies a universal nature of transport of holes within the oxide with respect to temperature, electric field and oxide thickness. The process is activated by an electric field and thermally activated above 140 K [9]. The microscopic transit times for individual carriers vary over many orders of magnitude. For our samples, the CV measurements were performed within six days of irradiation. While information regarding the time evolution of hole distribution within the oxide was lost during this elapsed time between irradiation and first characterization, we have since measured the CV curves again after an elapsed time of one year and report that all samples were consistent with previous measurements.

We have interpreted the shift in the flatband voltage, ΔV_{FB}, in terms of the electronic excitation caused in the oxide due to energetic ionic radiation. As shown in Fig. 2, ΔV_{FB} represents the horizontal shift in the irradiated C–V curve with respect to the pristine C–V curve. A charge distribution in the oxide bulk would result in a parallel shift of the C–V curve but would not induce a skew as observed in the irradiated C–V curves [23]. This parallel shift, in simple terms, is the additional voltage required to overcome the opposing electric field of the oxide-trapped charges. The skew, or equivalently the increased voltage range between accumulation and inversion, of the C–V curve is indicative of an increase in the interface trap density, D_{it}. The interface traps that lie outside the band gap are equivalent to charge trapped in the oxide, however the occupancy of the interface traps within the band gap changes with band bending at the interface. The interface traps are charged or neutral depending upon whether they are above or below the Fermi level. Since the Fermi level is shifting depending upon the applied gate voltage, the interface charge density varies with gate

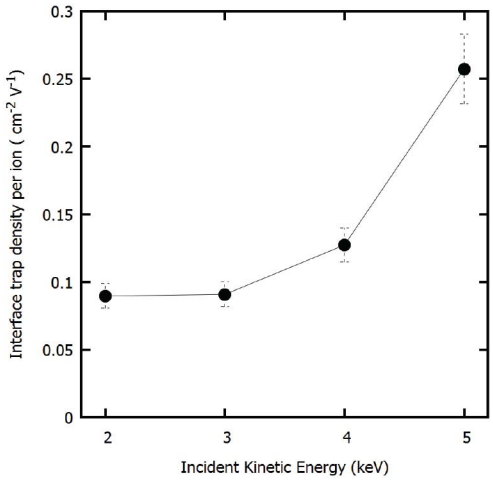

Fig. 7. $D_{\rm it}$ calculated per ion from the difference in $C_{\rm LF}$ and $C_{\rm HF}$ as a function of the kinetic energy of the incident ions.

voltage. It is this voltage-dependent charge at the interface that leads to the observed skew. The irradiated C–V curves shown in Fig. 3 show a distinctive increasing skew with increasing kinetic energy.

To quantify the interface state density, we have measured the response of the interface states to variable frequency gate-biasing. Specifically, the application of high frequency (HF) and low frequency (LF) biasing during the C–V acquisition results in a different effective capacitance for the MOS capacitor [4]. Under an applied low frequency bias the populated interface traps respond to give an additional capacitance, $C_{\rm it}$, that appears in parallel to that of the silicon substrate, $C_{\rm s}$. Therefore, the effective capacitance at low frequencies, $C_{\rm LF}$, is $C_{\rm ox}$ in series with $(C_{\rm it}||C_{\rm s})$. For a high frequency applied bias, the interface traps are unable to respond quickly enough to the time-dependent signal and therefore do not contribute to the measured capacitance. Therefore, the high frequency capacitance, $C_{\rm HF}$, contains only the equivalent capacitance of $C_{\rm ox}$ and $C_{\rm s}$ in series. Using the two measured effective capacitance values, $C_{\rm LF}$ and $C_{\rm HF}$, we have extracted $C_{\rm it}$ for our devices from which the interface trap density, $D_{\rm it}$, is obtained by dividing out the elementary charge and averaging over a range of applied gate voltages that correspond to the Fermi level variation about the middle of the Si band gap [4]. Fig. 7 shows our $D_{\rm it}$ values normalized by dose and their dependence on the kinetic energy of the incident ions.

Given that the maximum depth of the implanted ions in these measurements was within the first 5–15 nm of the oxide, it is remarkable that we observe interface effects at a depth of 190 nm, as shown in Fig. 7. Similar results have been observed by Winokur *et al.* [24], [25], where interface state effects were measured for both penetrating gamma rays and nonpenetrating UV radiation. In this case, the interface states are inferred to be created by transport of radiation-excited holes across the oxide. From the dose-normalized data in Fig. 7, we observe a superlinear dependence of $D_{\rm it}$ on the incident kinetic energy with $D_{\rm it}$ values ($\sim (6-20)\times 10^{11}$ cm^{-2} V^{-1}) that are similar in magnitude to the previous studies. It is reasonable therefore to interpret ions as an alternative form of nonpenetrating radiation, though further measurements are necessary to elucidate the full dependence of $D_{\rm it}$ on the ion impact conditions. We do note, however, that our assumption of a steady state solution for n_p in (4) has been tested using measurements of irradiated devices that were stored for over a year, and in all cases, the results reported here were reproduced. The reversibility of our ion-induced radiation damage was also verified by annealing the targets at $\sim 250^{\circ}$C, a result which is consistent with other radiation effects studies [6], [23].

IV. Summary

We have measured kinetic energy dependent irradiation effects of focused Na^+ ion beams on thick SiO_2 films ($\sim$ 1900 Å) on a Si substrate in the low energy regime (2–5 keV). These effects were encapsulated by depositing top metal contacts on irradiated and unexposed parts of the samples and comparing the C–V data obtained from the resulting individual MOS capacitors. An approximately linear relationship between the kinetic energy of the incident ions and shifts in the flatband voltages of the irradiated devices was observed in these measurements. The measured $V_{\rm FB}$ shifts were significantly ($\sim$ 3 times) larger than the values calculated and assigned to the presence of the implanted Na^+ ions, and the residual shift was attributed to subsurface electronic excitations caused by the passage of the ions into the oxide. These ion-induced excitations involve the dissipation of the ion kinetic energy to the electronic subsystem of the target and the generation of electron-hole pairs. Using the SRIM code the range of implantation of the ions within the oxide was calculated and used along with the electronic component of the stopping power to determine an expected density of generated holes. Within the columnar recombination model, it was shown that the subsequent transport and trapping of these holes will lead to a steady-state, uniform hole distribution in the oxide. A comparison of this expected trap density with that required to give the measured $V_{\rm FB}$ shifts shows a linear relationship that we use to infer a fractional yield of $\sim 1\%$ for hole survival. Interface trap states at the oxide-semiconductor interface are observed even though the ions are implanted only within the top 10% of the depth of the oxide. The density of the observed interface traps is calculated to be in the $\sim 10^{11}$ cm^{-2} V^{-1} range and a superlinear dependence on kinetic energy is observed. The results for hole survival and density of interface traps as well as the long term stability and annealing behavior of the irradiated oxides is consistent with results found under other forms of radiation [5]–[7], [9], [10], [17], [23]–[25], and overall, these measurements show that MOS devices can be used to track subsurface energy dissipation for impacting ions.

Acknowledgment

The authors would like to thank S. Chambers for his assistance in the characterization of MOS devices.

References

[1] S. Akcoeltekin, E. Akcoeltekin, T. Roll, H. Lebius, and M. Schleberger, "Patterning of insulating surfaces by electronic excitation," *Nucl. Instrum. Meth. B*, vol. 267, no. 8–9, pp. 1386–1389, Jun. 2009.

[2] F. Krok, S. R. Saeed, M. Kolmer, and M. Szymonski, "Patterning of ionic insulator surfaces with low-energy ion beams," in *Nanofabrication by Ion-Beam Sputtering Fundamentals and Applications*, D. Kanjilal, Ed. Stanford, CA, USA: Pan Stanford, 2012, ch. 4, pp. 109–134.

[3] R. E. Lake, J. M. Pomeroy, H. Grube, and C. E. Sosolik, "Charge state dependent energy deposition by ion impact," *Phys. Rev. Lett.*, vol. 107, no. 6, Jun. 2011, Art.ID 063202.
[4] E. H. Nicollian and J. R. Brews, *MOS (Metal Oxide Semiconductor) Physics and Technology*. Hoboken, NJ, USA: Wiley-Interscience, 1982.
[5] H. L. Hughes, "Surface effects of space radiation on silicon devices," *IEEE Trans. Nucl. Sci.*, vol. NS-12, no. 6, pp. 53–63, Dec. 1965.
[6] E. H. Snow, A. S. Grove, and D. J. Fitzgerald, "Effect of ionization radiation on oxidized silicon surfaces and planar devices," *Proc. IEEE*, vol. PROC-55, no. 7, pp. 1168–1185, Jul. 1967.
[7] T. R. Oldham and J. M. McGarrity, "Ionization of SiO_2 by heavy charged particles," *IEEE Trans. Nucl. Sci.*, vol. NS-28, no. 6, pp. 3975–3980, Dec. 1981.
[8] T. R. Oldham, "Recombination along the tracks of heavy charged particles in SiO_2 films," *J. Appl. Phys.*, vol. 57, no. 8, pp. 2695–2702, Apr. 1985.
[9] T. R. Oldham and F. B. McLean, "Total ionizing dose effects in MOS oxides and devices," *IEEE Trans. Nucl. Sci.*, vol. 50, no. 3, pp. 483–499, Jun. 2003.
[10] D. M. Fleetwood, "Total ionizing dose effects in MOS and low-dose-rate-sensitive linear-bipolar devices," *IEEE Trans. Nucl. Sci.*, vol. 60, no. 3, pp. 1706–1730, Jun. 2013.
[11] N. J. Chou and B. L. Crowder, "Effect of O^+ and Ne^+ implantation on the surface characteristics of thermally oxidized Si," *J. Appl. Phys.*, vol. 41, no. 4, pp. 1731–1738, Mar. 1970.
[12] K. G. Aubuchon, "Radiation hardening of P-MOS devices by optimization of the thermal SiO_2 gate insulator," *IEEE Trans. Nucl. Sci.*, vol. NS-18, no. 6, pp. 117–125, Dec. 1971.
[13] B. Deal, "The current understanding of charges in the thermally oxidized silicon structure," *J. Electrochem. Soc.*, vol. 121, no. 6, pp. C198–C205, Dec. 1974.
[14] G. F. Derbenwick and B. L. Gregory, "Process optimization of radiation-hardened CMOS integrated circuits," *IEEE Trans. Nucl. Sci.*, vol. NS-22, no. 6, pp. 2151–2156, Dec. 1975.
[15] D. McCaughan, C. White, R. Kushner, and D. Simms, "Differences in sodium transport in SiO_2 films caused by ion and neutral-particle bombardment," *Appl. Phys. Lett.*, vol. 35, no. 5, pp. 405–407, Sep. 1979.
[16] D. McCaughan, R. Kushner, D. Simms, and C. White, "Effects of bombardment by low-energy neutral particles on silicon dioxide films," *J. Appl. Phys.*, vol. 51, no. 1, pp. 299–304, Jan. 1980.
[17] R. J. Powell and G. Derbenwick, "Vacuum ultraviolet radiation effects in SiO_2," *IEEE Trans. Nucl. Sci.*, vol. NS-18, no. 6, pp. 99–105, Dec. 1971.
[18] J. F. Ziegler, J. P. Biersack, and U. Littmark, in *The stopping and range of ions in matter*, Elmsford, Pergamon, NY, USA, 1985.
[19] M. P. Ray, R. E. Lake, S. A. Moody, V. Magadala, and C. E. Sosolik, "A hyperthermal energy ion beamline for probing hot electron chemistry at surfaces," *Rev. Sci. Instr.*, vol. 79, Jul. 2008, Art. ID 076106.
[20] R. Shyam, "Energy loss of ions implanted in MOS dielectric films," Ph.D. dissertation, Dept. Phys. Astr., Clemson Univ., Clemson, SC, USA, Aug. 2014.
[21] S. M. Sze and K. K. Ng, *Physics of Semiconductor Devices*, 3rd ed. Hoboken, NJ, USA: Wiley–Interscience, 2007.
[22] G. A. Ausman and F. B. McLean, "Electron-hole pair creation energy in SiO_2," *Appl. Phys. Lett.*, vol. 26, no. 4, pp. 173–175, Feb. 1975.
[23] T. P. Ma and P. V. Dressendorfer, *Ionizing Radiation Effects in MOS Devices and Circuits*, ser. Wiley–Interscience. Hoboken, NJ, USA: Wiley, 1989.
[24] P. S. Winokur and M. M. Sokoloski, "Comparison of interface-state buildup in MOS capacitors subjected to penetrating and nonpenetrating radiation," *Appl. Phys. Lett.*, vol. 28, no. 10, pp. 627–630, May 1976.
[25] P. Winokur, J. McGarrity, and H. Boesch, "Dependence of interface-state buildup on hole generation and transport in irradiated MOS capacitors," *IEEE Trans. Nucl. Sci.*, vol. NS-23, no. 6, pp. 1580–1585, Dec. 1976.